Robot-Assisted FBG-based Sensorized Needle Calibration

Paper Seminar Report

EN 601.656 Computer Integrated Surgery II

Kefan Song

M.S.E student, Biomedical Engineering Department

ksong13@jhu.edu

1. Project Summary

The objective of the project is to calibrate flexible needles with FBG-based shape-sensing capabilities that are going to be used for prostate biopsy and brachytherapy procedures. When performing these procedures, a new approach, which consists of inserting a flexible needle with robotic assistance under real-time MRI guidance, was shown to have better accuracy and repeatability than the current standard approach (Seifabadi, 2012). However, the flexible needles need to be calibrated on an individual basis to largely reduce the error in sensing the shape of the needle, and current calibration process is done by hand. As the needles are very sensitive, manual needle calibration is very time-consuming and prone to human error. Thus the specific aim of this project is to develop an automatic needle calibration process that can be both precise and efficient.

2. Paper Selection

The paper selected is "Improved FBG-Based Shape Sensing Methods for Vascular Catheterization Treatment" published in 2020 by Omar Al-Ahmad *et al*. The reason behind choosing this paper is that this paper also focuses on the calibration of an FBG-based shape sensing mechanism even though it was integrated onto a catheter instead of a needle. This paper also has a detailed explanation of the working mechanism of FBG sensors as well as possible sources of error, thus it serves as a good introductory paper to projects related to shape sensing using fiber optics.

3. Summary

This paper mainly discusses the methods for fiber integration within catheters to improve shape estimation accuracy and repeatability. It also introduces a two-step calibration process for intrinsic twist compensation and a practical method for fiber parameter identification. An example calibration setup was then demonstrated and validated.

4. Paper Content

This paper is divided into six sections. The first section serves as an introduction to the topic; the second section covers the basic principles and algorithms related to FBG sensing and shape reconstruction; the third section focuses on the main factors that contribute to shape accuracy; the fourth section introduces the experimental setup and method of this study with the experimental results discussed in the fifth section; the last section gives the conclusion and future directions of the project.

<u>Introduction</u>

This paper started with an introduction to the history and prior work in the field of Fiber optic shape sensing (FOSS). FOSS was introduced several decades ago and have since been used frequently due to its advantages as a shape sensor, which includes electromagnetic immunity, miniature size, high interrogation speed, multiple sensing points, and so on. Two commonly used techniques with regards to fiber strain sensing are Fiber Bragg Gratings (FBGs) and Rayleigh scattering, and two main interrogation

technologies are Optical Frequency Domain Reflectometry (OFDR), which is mainly used with Rayleigh scattering based techniques, and Wavelength Division Multiplexing (WDM), which is commonly used on FBG-based techniques. In terms of the reconstruction methods, these are commonly based on Frenet-Serret frames, parallel transport or Bishop frames, constant curvature segmentation, and helical geometry. A table that summarizes prior shape sensing research and corresponding shape accuracy errors was also provided (Table 1).

TABLE I
SHAPE SENSING EXAMPLES FROM PREVIOUS LITERATURE (ALL DIMENSIONS ARE IN MILLIMETRE)

Authors	Interrogation	Fibers & Cores	Conf.	Model	Length	#Grts	Spacing	Validation	Error	R_{min}
Abayazid *et al.* [11]	FBG / WDM	3 outer / no central	Straight	Constant curvature	90	4	30	2D / 3D	2.10 ± 1.10 (mean)	375
Henken *et al.* [12]	FBG / WDM	3 outer / no central	Straight	Frenet-Serret	70	2	70	2D	1.32 ± 0.48 (mean)	NA
Yi *et al.* [23]	FBG / WDM	4 outer / no central	Straight	Frenet-Serret	400	5	100	2D / 3D	4.10 (mean)	NA
Elayaperumal *et al.* [24]	FBG / WDM	3 outer / no central	Straight	Other	85	2	85	2D	4.20 (rms)	NA
Gander *et al.* [25]	FBG / WDM	4 (MCF) / no central	Straight	Other	NA	NA	NA	2D	2.00 (max)	20
Van de Berg *et al.* [13]	FBG / WDM	3 outer / no central	Straight	Frenet-Serret	120	4	40	3D	2.60 ± 1.10 (mean)	71.4
Parent *et al.* [26]	OFDR	3 outer / no central	Straight	Other	NA	NA	NA	2D	≈1.00 (rms)	17.5
Sefati *et al.* [14]	FBG / WDM	3 outer / no central	Straight	Constant curvature	NA	NA	NA	3D	0.62 (max)	101.6
Ryu *et al.* [17]	FBG / WDM	3 outer / no central	Straight	Other	NA	NA	NA	2D	0.84 ± 0.62 (mean)	NA
Leyendecker *et al.* [27]	FBG / WDM	3 (MCF) / central	Straight	Constant curvature	250	6	50	2D / 3D	15.40 (max)	NA
Lally *et al.* [28]	OFDR	3 (MCF) / central	Helical	Other	30000	NA	NA	3D	210 (max)	NA
Klute *et al.* [1]	OFDR	3 outer / no central	Straight	Constant curvature	2000	NA	NA	3D	42.9 (max)	14
Duncan *et al.* [10]	OFDR	3 (MCF) / no central	Straight	NA	1100	110	10	2D	22.50 ±0.5 (max)	667
Khan *et al.* [29]	FBG / WDM	4 (MCF) / no central	Straight	Frenet-Serret	108	6	18	2D / 3D	1.05 (max)	NA
Roesthuis *et al.* [18]	FBG / WDM	3 outer / no central	Straight	Frenet-Serret	90	4	3	2D	1.14 (mean)	30
Kim *et al.* [15]	FBG / WDM	3 outer / no central	Straight	Constant curvature	150	NA	NA	3D	0.53 (max)	NA
Wang *et al.* [30]	FBG / WDM	4 outer / no central	Straight	Frenet-Serret	200	5	50	3D	15.00 (mean)	NA
Moore *et al.* [2]	FBG / OFDR	3 (MCF) / no central	Straight	Frenet-Serret	1100	111	10	3D	31.06 (max)	14.3
Roesthuis *et al.* [4]	FBG / WDM	3 outer / no central	Straight	Constant curvature	90	4	30	2D / 3D	1.66 (max)	15

Then it moves on to discussing the major factors that influences the reconstruction accuracy of the shape sensing schemes. These include the interrogation method, the quality of fiber integration, the calibration and parameter identification processes, the twist compensation mechanism and the reconstruction algorithm. This section ends with a general statement of the contributions provided in this paper: a fiber integration approach into a catheter, a two-step calibration method for intrinsic twist, a new approach for spatial curve reconstruction based on Helical Extension Method (HEM), a parameter identification method, and the validation process of all these methods.

Basic Principles

This section mainly walks through the derivations of major equations involved in the shape sensing mechanism as well as the shape reconstruction algorithm, and all equations mentioned are listed in Figure 2. In this paper, all algorithms and equations apply to the multi-core fibers (MCFs), which has a central core and a number of symmetrically positioned outer cores, as shown in Figure 1. For the equations, equation 1 is the main function behind the FBG sensor as it connects the strain ϵ with curvature κ, whereas equation 2 and 3 are used for MCFs to measure the change of strain measured by each outer core. Equation 4 describes the relationship between the strain of each core ϵ_i and the curvature κ according to the geometry shown in Figure 1 (a), and the equation set 5 is used to obtain a closed-form solution for the curvature κ and the bend angle θ_b. With respect to the shape reconstruction algorithm, a set of the curve's tangent $\boldsymbol{T}$, normal $\boldsymbol{N}$ and binormal $\boldsymbol{B}$ unit vectors can be obtained from its curvature κ and torsion τ profiles using Frenet-Serret formulae, in which the torsion profile τ is the derivative of the bend angle, and the Cartesian position of the curve can be obtained using equation 6.

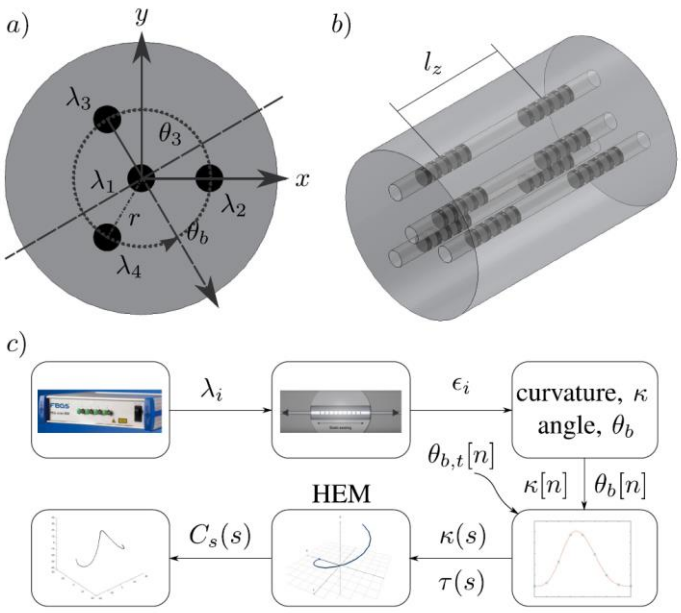

Figure 1. a) Cross-sectional view of a 4 core MCF, b) isometric view of a short segment with 4 cores and 2 FBG sets, c) flowchart of reconstruction algorithm.

$$\epsilon = -\kappa y \tag{1}$$

$$\frac{\lambda_B - \lambda_{B_0}}{\lambda_{B_0}} = \frac{\Delta\lambda_B}{\lambda_{B_0}} = S_\epsilon \Delta\epsilon + S_T \Delta T \tag{2}$$

$$\Delta\epsilon_i = \frac{\Delta\lambda_{B,i}}{S_\epsilon \lambda_{B_0,i}} - \frac{\Delta\lambda_{B,1}}{S_\epsilon \lambda_{B_0,1}} \tag{3}$$

$$\epsilon_i = -\kappa r \sin(\theta_b - 3\pi/2 - \theta_i) \tag{4}$$

$$\boldsymbol{\kappa}_{app} = -\sum_{i=1}^{N} \frac{\epsilon_i}{r} \cos\theta_i \hat{\boldsymbol{i}} - \sum_{i=1}^{N} \frac{\epsilon_i}{r} \sin\theta_i \hat{\boldsymbol{j}}$$

$$\kappa = \frac{2|\boldsymbol{\kappa}_{app}|}{N},$$

$$\theta_b = \angle\boldsymbol{\kappa}_{app}, \tag{5}$$

$$C_s(s) = C_{s,0} + \int_0^l \boldsymbol{T}(s) ds \tag{6}$$

Figure 2. Major equations presented in the Basic Principles section.

Contributors to Shape Accuracy

In this section some major contributors to the reconstructed shape accuracy of the FBG sensors are discussed. These include the interrogation method, the fiber integration method, the presence of twist compensation, calibration for twist compensation, parameter identification, and the reconstruction algorithm.

- Interrogation method

  As mentioned before, WDM and OFDR are the most popular interrogation methods, and they have different traits that allow them to be used for different purposes. OFDR can provide extremely high spatial resolutions, but its refresh rates are not as high, and it's also more expensive in commercial cost. WDM, on the other hand, is not as accurate, but can collect data at a much higher frequency with higher signal-to-noise ratio. OFDR also has lower wavelength measurement accuracy compared to WDM.

- Fiber integration

  A method of integrating an MCF into a conventional catheter is proposed in this section, as shown in Figure 3. The major guidelines of the integration method include reducing the spacing between the MCF and the inner lumen of the catheter, including one or two rigid fixations at the base of the MCF with distance Δx_{prox} to the closest FBG grating, and attaching the MCF at a location where its tip is at distance Δx_{dist} away from the tip of the catheter.

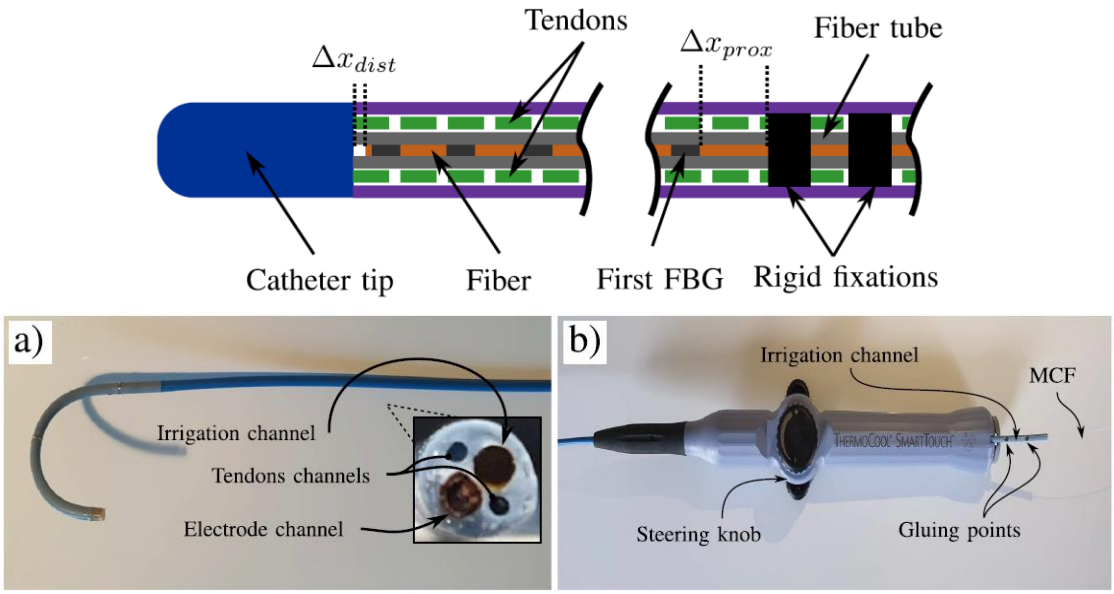

Figure 3. Proposed integration method of an MCF into a conventional catheter.

- Twist compensation

  The fiber twist has always been an issue in fiber-based shape sensing because the sensor is much more sensitive in sensing the strain caused by the twist. Several methods are proposed to prevent the twist, but an observation was made by the authors that MCF fibers exhibit an intrinsic twist even when they are externally unloaded. Thus having some sort of twist compensation mechanism in the mechanical design is necessary and should be considered.

- Calibration for twist compensation

  A two-step calibration process is proposed to account for the fiber twist inside the catheter, as shown in Figure 4. In order to calibrate a catheter, it is first positioned in a straight line with no externally induced forces (Figure 4 left). The FBG wavelengths are recorded as reference wavelengths. Next, it is bent on a flat surface so that the catheter is under curvature. Using equations 3~5, the bending angles due to intrinsic twist can be computed. These angles are constant and are part of the unique properties of the catheter being calibrated. The calibrated bending angle used for shape reconstruction will be its raw data minus the bending angles due to the intrinsic twist.

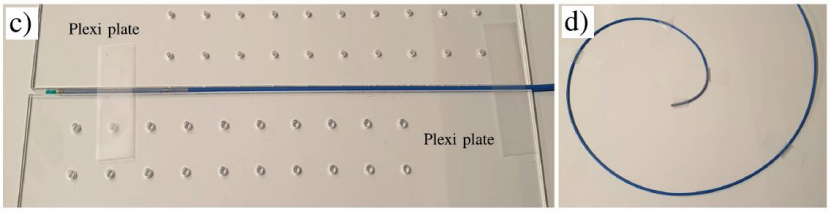

Figure 4. Steps one (left) and two (right) of the calibration process.

- Parameter identification

  Each MCF sensor comes with a set of input parameters that are needed for the shape reconstruction model to work accurately. It has been observed that slight deviations of some of the parameters can lead to changes on the final estimation accuracy. However, even though these parameters are provided by the MCF manufacturers, these parameters are often averaged value and not tailored to each individual sensor. Thus, a procedure was proposed to provide an estimation of the model parameters. To estimate the parameters of the catheter, it is positioned in a variety of 2D or 3D shapes with known ground truth, which means that with each configuration there would be a curve $C_{s,gr}(s)$ describing the ground truth. Then, the parameters can be estimated by minimizing the cost function shown in Figure 5 using Iterative Closest Point algorithm.

$$\boldsymbol{C}(\boldsymbol{\Theta}) = \sum_{i=1}^{k} \max(\, \boldsymbol{d}(C_{s,gr}(s,k) - C_{s,rc}(s,k,\boldsymbol{\Theta})))$$

for $\boldsymbol{\Theta}$ subject to

$$\begin{cases} \boldsymbol{\Theta} = [\Delta\theta,\ r,\ S_\epsilon], \\ \Delta\theta_{\min} \le \Delta\theta \le \Delta\theta_{\max}, \\ r_{\min} \le r \le r_{\max}, \\ S_{\epsilon,\min} \le S_\epsilon \le S_{\epsilon,\max}, \end{cases}$$

Figure 5. Cost function associated with the MCF sensor parameters.

- Reconstruction algorithm
  To improve shape accuracy, three modifications are proposed in the reconstruction algorithm. The first one is to code for twist compensation, which was previously mentioned, the second modification is to construct the spatial curve using the Helical Extension Method, and the third modification is to compare different interpolation techniques and employ one with the best performance.

Experimental Setup

The experimental setup for the FBG needle was divided into two parts: static tests and dynamic tests. For the static tests, six 2D shapes and six 3D shapes with known ground truth curves are printed (Figure 6 a), with half of each configuration used for parameter optimization and the other half for validation. The catheter was then inserted into the different shapes to be calibrated using the method proposed in the previous section. Each insertion was repeated five times, and in total 30 trials are used for optimization with the other half used for validation. The effect of temperature variation was also investigated by submerging the catheter into a hot water bath while monitoring the tip position and the water temperature (Figure 6 b).

For the dynamic tests, an EM sensor was fixed to the tip of the catheter. The catheter was then rotated to measure the effect of longitudinal catheter rotation. After that, it was inserted into and pulled out of a sheath multiple times to measure its repeatability. The effect of tendon actuation was measured by actuating the tip of the catheter for several times while the catheter was inserted in the sheath, and the effect of dynamic catheter movement was measured by manually moving the catheter through the sheath without any lubrication.

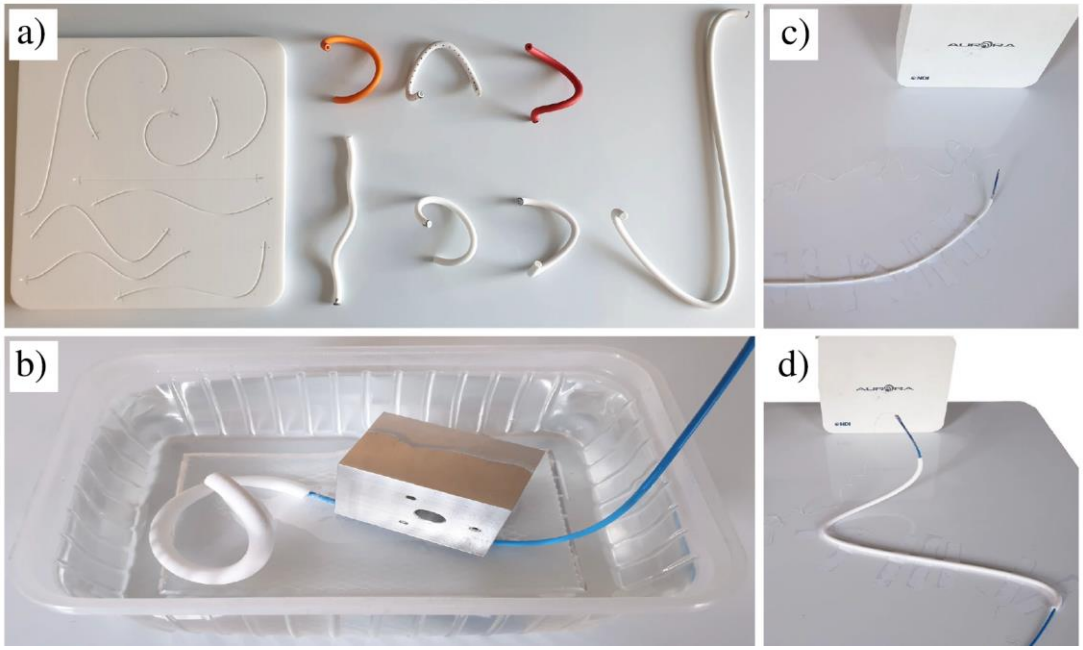

Figure 6. Experimental setup for the FBG catheter calibration.

Results

Figures 7 and 8 shows the results of the experiment. Figure 7 shows that the optimized parameters have a distinguishable variation compared to the provided parameters, and that calibrating for twist compensation effectively improves the accuracy of the reconstruction model. Figure 8a shows that the variation caused by temperature is mostly uniform and are almost negligible. Figure 8b shows that the rotation induces negligible twist and has no major effect on shape accuracy, as the reconstructed curve coincide after registration of curves in different rotation angles. Figure 8c shows that the catheter demonstrates excellent repeatability even without lubrication, and the result will probably be better in real-life scenarios. Figure 8d shows that the shape reconstruction is not affected by tendon actuation, and figure 8e shows that the distance error increases when there's sharp bends in the dynamic model. However, this type of error could be mitigated by applying lubrication in the sheath, and to use larger FBG spacing to avoid wavelength overlap in the spectrum.

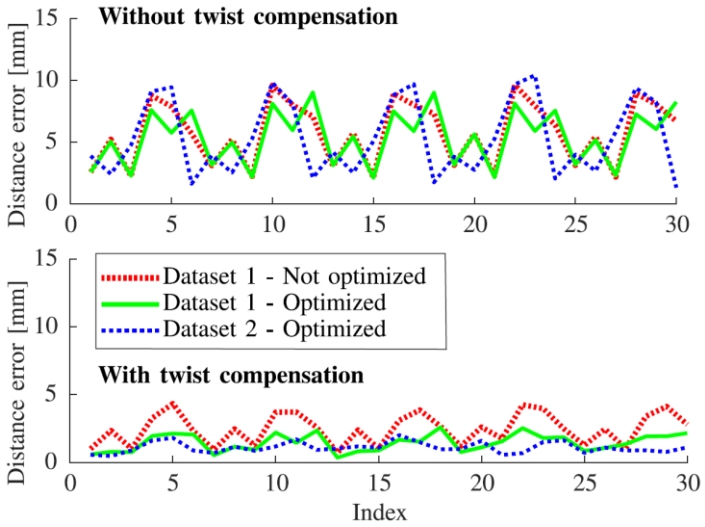

Figure 7. Maximum distance errors between the ground truth and reconstructed curves using original and optimized model parameters.

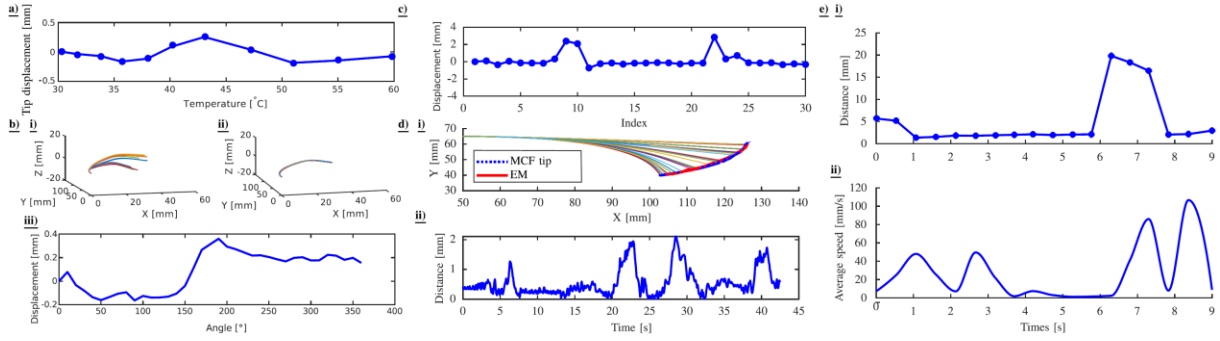

Figure 8. (a) tip displacement of a static catheter versus temperature, (b) effect of catheter rotation along its longitudinal axis on tip position: i) shapes pre registration, ii) shape post registration, iii) tip displacement from a reference point for different rotation angles, (c) displacement of the catheter's tip from a reference point for different trials, (d) effect of tendons on reconstructed shape and comparison of tip position between MCF reconstruction and EM sensor, (e) maximum distance error between the shapes of the moving catheter and 3D printed sheath.

Conclusion

This paper explored the effect of multiple factors on the accuracy of shape reconstruction of an FBG-based catheter. It also proposed several different algorithms to mitigate the possible errors. Through experiment, it shows that when applying these calibration algorithms, the FBG-based catheter is able to reconstruct the shape pretty accurately.

5. Critique (Pros & Cons)

Despite being really detailed about the algorithms and mechanisms of the FBG-based catheter, this paper is really easy to follow as it is nicely structured with clear diagrams. The explanations to the equations are also nicely constructed, with clearly stated connections between equations. Also, this paper constructed a really detailed calibration experiment, which can be applied to many different cases, including the case of my current project.

The one thing that this paper was missing in its experiment is a preliminary step to classify whether the FBG sensors are working properly. From the experiences of my fellow researchers in the lab, the FBG fibers are somewhat fragile, and it usually doesn't have any visible damage even though it is faulty. Thus, a preliminary step to ensure that the needle is working properly seems important, especially since the experiment setup in the paper involves a lot of different measurements and setups.

6. Takeaways

This paper can serve as a general guidance in using the FBG sensor for shape reconstruction. The FBG-based needle that I am working on can be considered as a shorter and much more rigid catheter, so a lot of principles are still applicable in my project. Also, it is a good reference to compare my own calibration setup to, and see whether there are more factors that needed to be calibrated in the calibration process that I designed.

7. References

Seifabadi, R., Iordachita, I., & Fichtinger, G. (2012, June). Design of a teleoperated needle steering system for MRI-guided prostate interventions. In 2012 *4th IEEE Ras & Embs International Conference on Biomedical Robotics And Biomechatronics (Biorob)* (pp. 793-798). IEEE.

Al-Ahmad, O., Ourak, M., Van Roosbroeck, J., Vlekken, J., & Vander Poorten, E. (2020). Improved FBG-Based Shape Sensing Methods for Vascular Catheterization Treatment. IEEE Robotics and Automation Letters, 5(3), 4687-4694.